Обзор ArXiv/astro-ph, 11-16 мая 2023 года

От Сильченко О.К.

ArXiv: 2305.05709

NGC 1436: the making of a lenticular galaxy in the Fornax cluster

Alessandro Loni,[1,2]★ Paolo Serra,[2] Marc Sarzi,[1] Gyula I. G. Józsa,[3,4] Pablo M. Galán–de Anta,[1,5] Nikki Zabel,[6] Dane Kleiner,[7,2] Filippo M. Maccagni,[7,2] Daniel Molnár,[2] Mpati Ramatsoku,[4,2] Francesca Loi,[2] Enrico M. Corsini,[8,9] D. J. Pisano,[6] Peter Kamphuis,[10] Timothy A. Davis,[11] W. J. G. de Blok,[7,12,13] Ralf J. Dettmar,[10] Jesus Falcon-Barroso,[14,15] Enrichetta Iodice,[16] Maritza A. Lara-López,[17] S. Ilani Loubser,[18] Kana Morokuma-Matsui,[19] Reynier Peletier,[12] Francesca Pinna,[20] Adriano Poci,[21] Matthew W. L. Smith,[11] Scott C. Trager,[12] and Glenn van de Ven[22]

[1]*Armagh Observatory and Planetarium, College Hill, Armagh BT61 9DG, UK*
[2]*INAF – Osservatorio Astronomico di Cagliari, Via della Scienza 5, 09047, Selargius, CA, Italy*
[3]*Max-Plank-Institut für Radioastronomie, Auf dem Hügel 69, 53121 Bonn, Germany*
[4]*Department of Physics and Electronics, Rhodes University, PO Box 94, Makhanda 6140, South Africa*
[5]*Astrophysics Research Centre, School of Mathematics and Physics, Queen's University Belfast, Belfast BT7 INN, UK*
[6]*Department of Astronomy, University of Cape Town, Private Bag X3, Rondebosch 7701, South Africa*
[7]*Netherlands Institute for Radio Astronomy (ASTRON), Oude Hoogeveensedijk 4, 7991 PD Dwingeloo, the Netherlands*
[8]*Dipartimento di Fisica e Astronomia "G. Galilei", Università di Padova, vicolo dell'Osservatorio 3, I-35122 Padova, Italy*
[9]*INAF - Osservatorio Astronomico di Padova, vicolo dell'Osservatorio 2, I-35122 Padova, Italy*
[10]*Ruhr University Bochum, Faculty of Physics and Astronomy, Astronomical Institute, 44780 Bochum, Germany*
[11]*School of Physics and Astronomy, Cardiff University, Queens Buildings The Parade, Cardiff, CF24 3AA, UK*
[12]*Kapteyn Astronomical Institute, University of Groningen, PO Box 800, NL–9700 AV Groningen, the Netherlands*
[13]*The Inter-University Institute for Data Intensive Astronomy, Department of Astronomy, University of Cape Town, Private Bag X3, Rondebosch, 7701, South Africa*
[14]*Instituto de Astrofísica de Canarias, Vía Láctea s/n, E-38205 La Laguna, Tenerife, Spain*
[15]*Departamento de Astrofísica, Universidad de La Laguna, E-38200 La Laguna, Tenerife, Spain*
[16]*INAF – Astronomical Observatory of Capodimonte, Salita Moiariello 16, 80131, Naples, Italy*
[17]*Departamento de Física de la Tierra y Astrofísica, Instituto de Física de Partículas y del Cosmos, IPARCOS. Universidad Complutense de Madrid (UCM), 28040, Madrid, Spain*
[18]*Centre for Space Research, North–West University, Potchefstroom 2520, South Africa*
[19]*Center for Computational Sciences, University of Tsukuba, Ten-nodai, 1-1-1 Tsukuba, Ibaraki 305-8577, Japan*
[20]*Max-Planck-Institut für Astronomie, Königstuhl 17, D-69117 Heidelberg, Germany*
[21]*Centre for Extragalactic Astronomy, University of Durham, Stockton Road, Durham DH1 3LE, United Kingdom*

Обман трудящихся в заголовке: NGC 1436-спиральная галактика

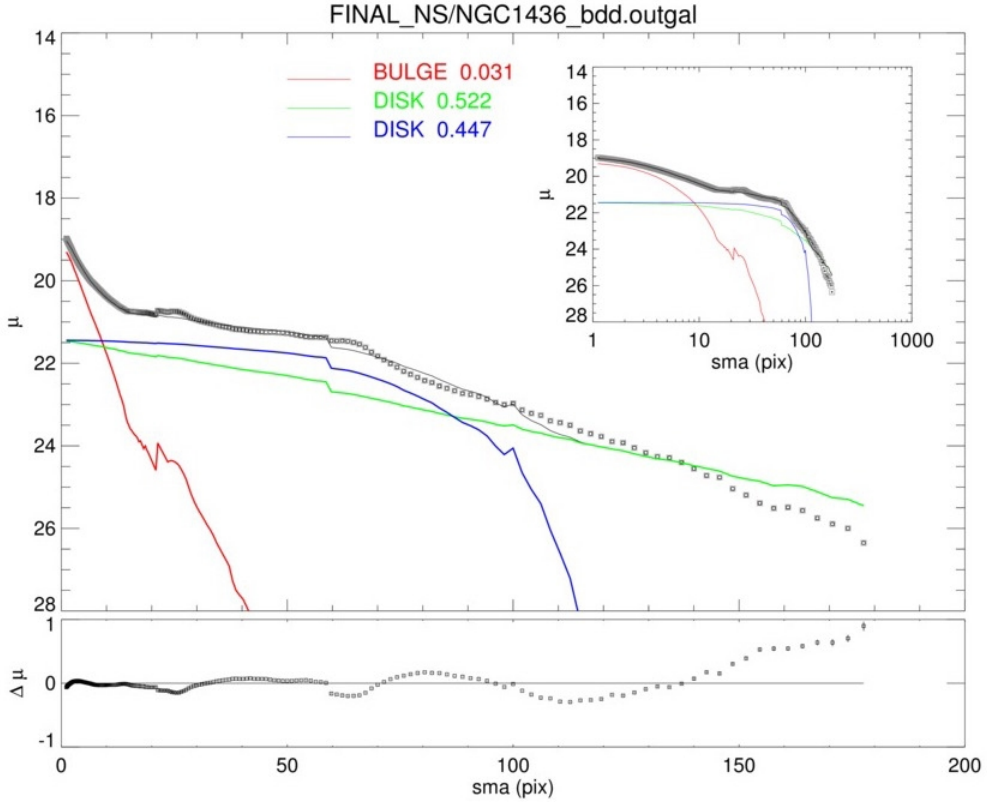

- (NED): (R')SAB(s)bc
- Вклад балджа в полную светимость – 3.1% (S4G) или 3.9% (R, Carnegie-Irwin)

… но в центре скопления Fornax

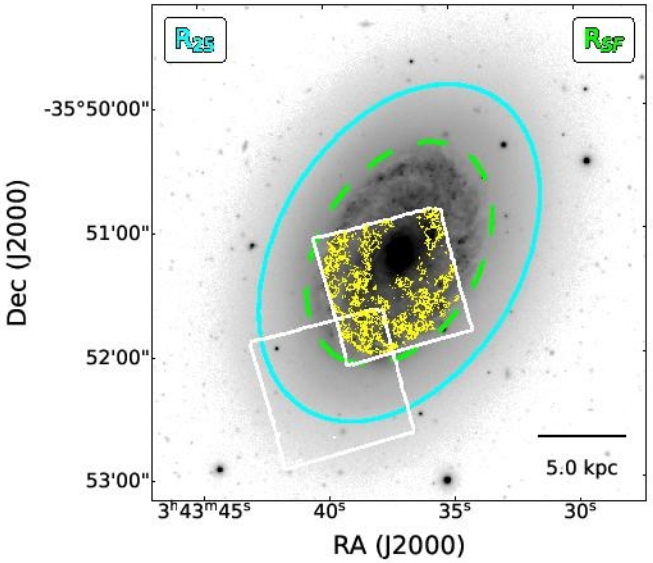

Figure 1. Optical g–band image of NGC 1436 from the Fornax Deep Survey (Peletier et al. 2020) showing the morphological distinction between the inner star-forming regions characterised by flocculent spiral features and the quiescent and smoother outer disc. The footprint of the Fornax3D observations for NGC 1436 (Sarzi et al. 2018) (white squares) and the map of the Hα emission detected in the MUSE data by Iodice et al. 2019b (yellow) are also shown. The latter measurements set the extent of the star-forming disc (R_{SF} 59 $''$, dashed green line), while the cyan isophotal radius measured at 25 mag arcsec^{-2} in B-band (de Vaucouleurs et al. 1991) gives an overall indication for the extent of NGC 1436.

2.1 MeerKAT

We study the distribution and kinematics of HI in NGC 1436 using data products from the MeerKAT Fornax Survey. The survey goals, design, observations and HI data processing are described in Serra et al. (2023). Here we make use of the HI subcubes and moment images of NGC 1436 at a resolution of 11$''$and 66$''$(see Table 2 in Serra et al. 2023). The 11$''$cube has a noise level of 0.28 mJy beam^{-1} and a 3σ HI column density sensitivity of 4.5×10^{19} cm^{-2}. The 66$''$cube has a noise level of 0.29 mJy beam^{-1} and a 3σ HI column density sensitivity of 1.3×10^{18} cm^{-2}. In both cases the column density sensitivity is calculated assuming a linewidth of 25 km s^{-1}. The spectral resolution of both cubes is 1.4 km s^{-1}.

2.2 ALMA

The ALMA observations of the ^{12}CO(1–0) line used in this work, whose data reduction is described in Zabel et al. (2021), consist of a combination of high resolution data from the ALMA Fornax Cluster Survey obtained with the 12-m configuration array (Zabel et al. 2019) and deep data from the ALMA archive (Morokuma-Matsui et al. 2022) obtained with the Atacama Compact Array. The final cube has a velocity resolution of 10 km s^{-1}, a synthesized beam size of 2.68$''$×2.06$''$, and a noise level of ~2.0 mJy beam^{-1}.

Новые данные

Как все спирали в скоплениях, обеднена газом

Using Eq. 50 in Meyer et al. (2017), we estimate the total $M_{\rm HI}$ to be $(1.9 \pm 0.2) \times 10^8$ $M_\odot$. Based on ATCA data, Loni et al. (2021) pointed out that NGC 1436 is a HI-deficient galaxy with a large $M_{\rm H_2}/M_{\rm HI}$ ratio. These results do not change if we use the MeerKAT $M_{\rm HI}$ value, which is 4σ larger than the ATCA one, the same $M_\star$ value calculated in Loni et al. (2021), and the $M_{\rm H_2}$ value by Zabel et al. (2021) (which is a factor ~1.4 smaller than that used in Loni et al. 2021 from Zabel et al. 2019). Indeed, (*i*) the offset between the $M_{\rm HI}/M_\star$ ratio of NGC 1436 and the xGASS $M_{\rm HI}$-$M_\star$ scaling relation (Catinella et al. 2018) is still larger than the RMS deviation of a sample of non-cluster galaxies (Kreckel et al. 2012; Boselli et al. 2014a) and (*ii*) the $M_{\rm H_2}/M_{\rm HI}$ ratio of NGC 1436 is 1.0±0.1, resulting ~ 12 σ above the xGASS weighted average of $\log_{10}(M_{\rm H_2}/M_{\rm H_I})$.

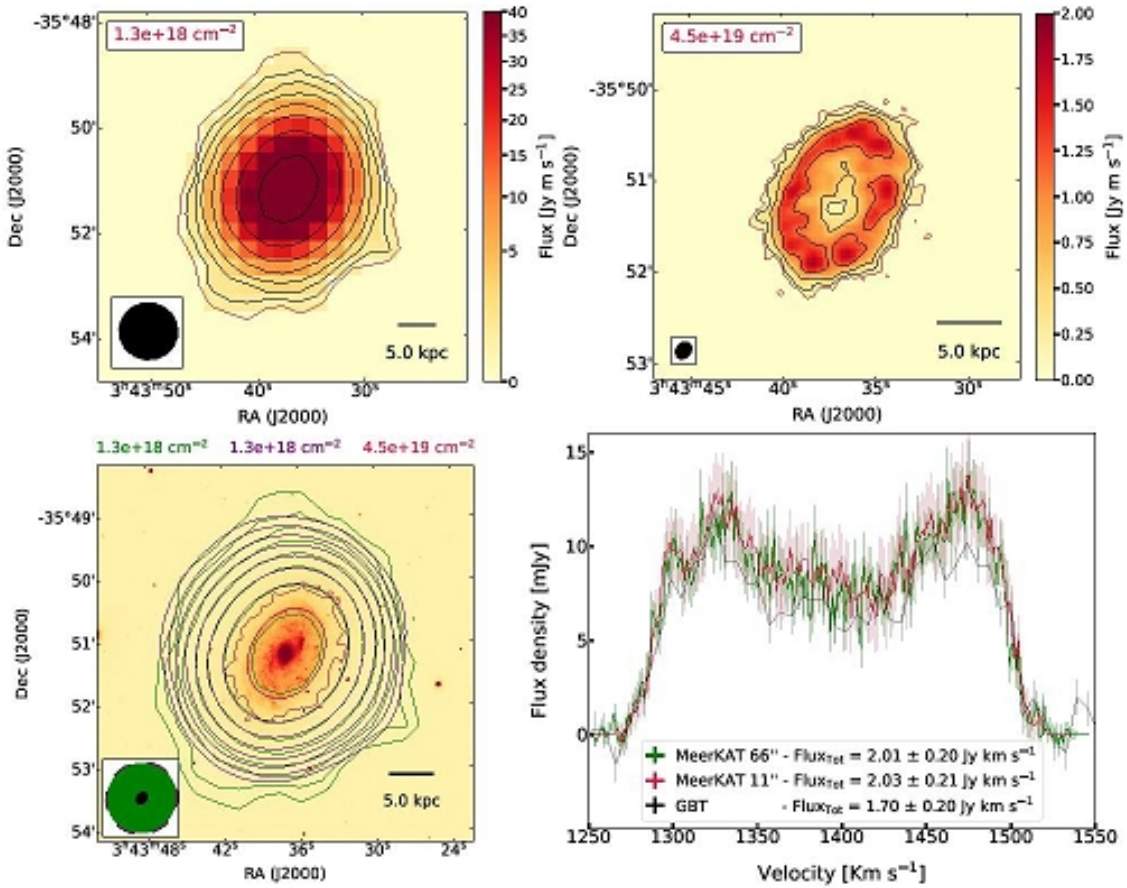

Figure 2. The top panels show the MeerKAT HI image at a resolution of 66″(left) and 11″(right). In each panel the value on the top left gives the level of the lowest HI contour (shown in red), which is calculated as the 3σ sensitivity over a 25 km s^{-1} line width. The HI contours increase by a factor of 2 at each step. The PSF and a 5 kpc scale bar are shown on the bottom-left and bottom-right corner, respectively. The bottom left panel shows with green, red and purple contours the (*1*) 66″HI image (*2*) lowest reliable contour of the 11″HI image (*3*) 11″image convolved to a 66″resolution. With the same colors we show the 3σ column density sensitivity of the respective HI image (top of the image) and their PSFs (bottom-left). The *g*-band optical image comes from the Fornax Deep Survey (Peletier et al. 2020). The bottom right panel shows spectra extracted from the 11″(red) and 66″(green) cubes, and from single-dish data (GBT, Courtois et al. 2009 - black), respectively. The legend shows the total fluxes obtained from these data. The uncertainties on the total MeerKAT fluxes are calculated by summing in quadrature the statistical uncertainties – derived from the local RMS and the number of independent pixels detected in each channel – and the 10% MeerKAT flux uncertainty measured in Serra et al. (2023). The spectral axis shows velocity in the optical convention.

Газовый диск не имеет диффузного протяжения

Регулярное круговое вращение

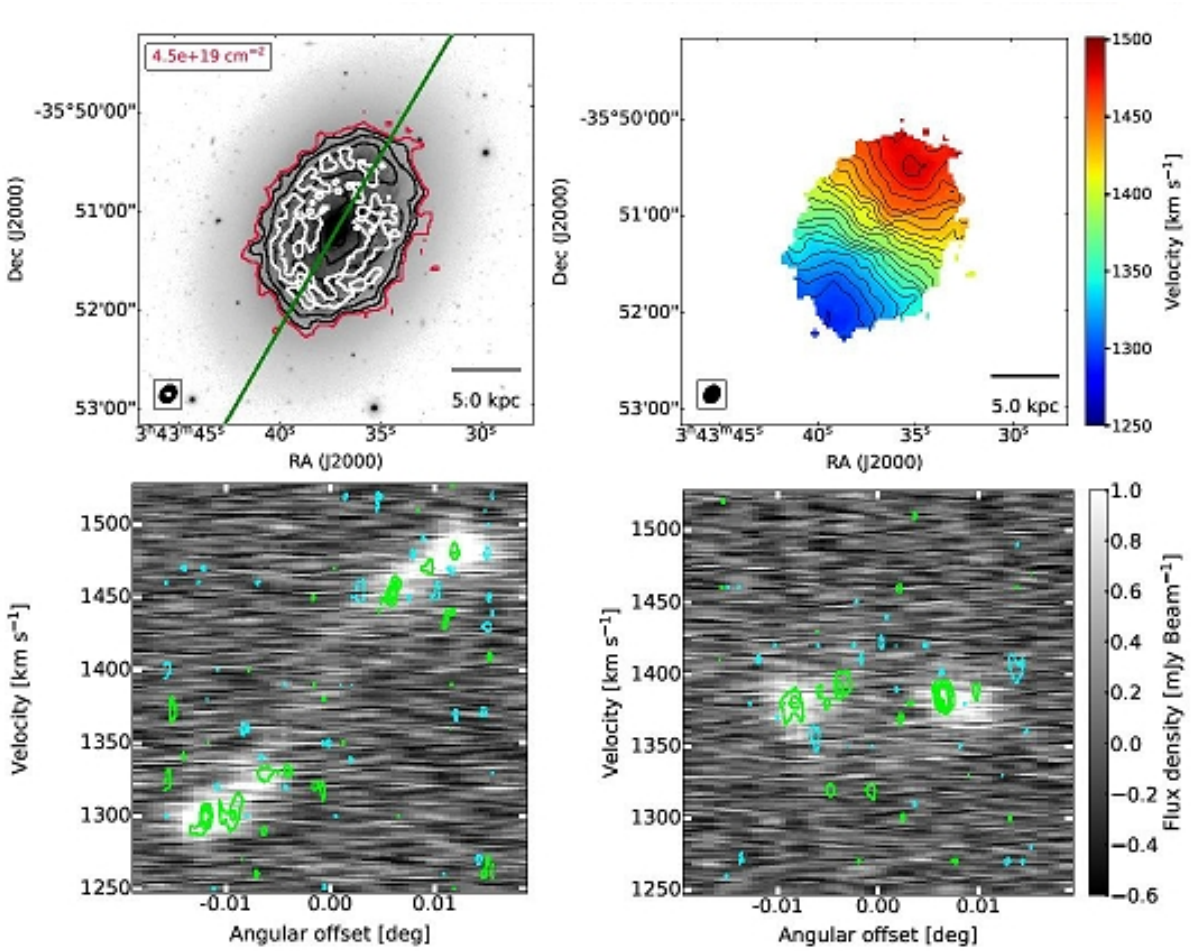

Figure 3. Top-left: comparison between the HI and CO gas distribution from the MeerKAT (red and black contours as in the top-right panel of Fig. 2) and ALMA (white contours) data, with corresponding beam sizes shown in the lower-left corner of this panel (in black and white, respectively). Bottom panels: comparison of the PV-diagram of HI and CO along the major axis (green line on the top left panel) and minor axis. The background image shows the HI while the green contours show the CO emission at 2.5σ, increasing in steps of 2. Cyan contours show the negative signal in the CO ALMA cube, whose absolute level is the same as that of the first positive green contour.

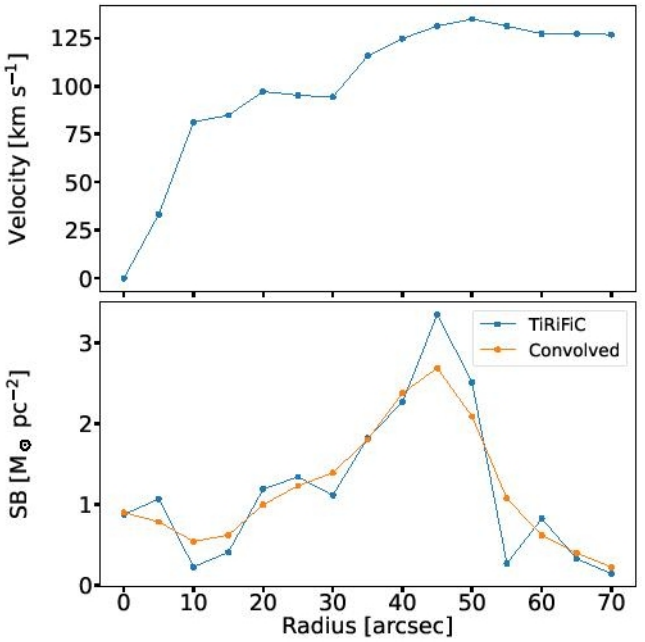

Figure 4. Results from tilted-ring analysis of the MeerKAT HI data, showing the TiRiFiC HI rotation curve (top panel) and HI surface-brightness profile (bottom panel). The latter shows clearly the abrupt transition towards the HI deficient and quiescent outer disc beyond a radius of 55″.

Восстановление истории звездообразования по данным MUSE

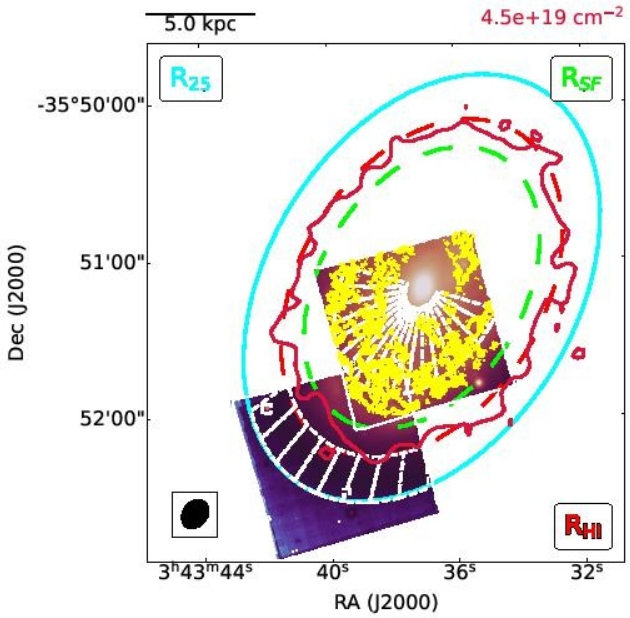

Figure 5. Comparison between the reconstructed MUSE image, MUSE Hα emission and the MeerKAT HI data for NGC 1436 informing the location of the MUSE aperture spectra used in our star-formation history analysis. As in Fig. 1 the cyan and green ellipses indicated, respectively, the isophotal level at 25 mag/arcsec^2 in B-band and the limit of the star-forming disc, where the Hα emission is traced by the yellow contours. The extent of the gas reservoir in NGC 1436 is traced here by the red contours for a limiting HI column density of 4.5×10^{19}cm^{-2}, which are best fitted by the shown red ellipse setting the radius of the HI disc at R_{HI} 70 $''$. Finally, the white dashed lines show the location of the annular sectors used to extract the aperture spectra in both the inner and outer disc for our SFH analysis, where the former avoid the bulge regions (inside 9$''$) and extend to the limit of the MUSE central

Восстановили…

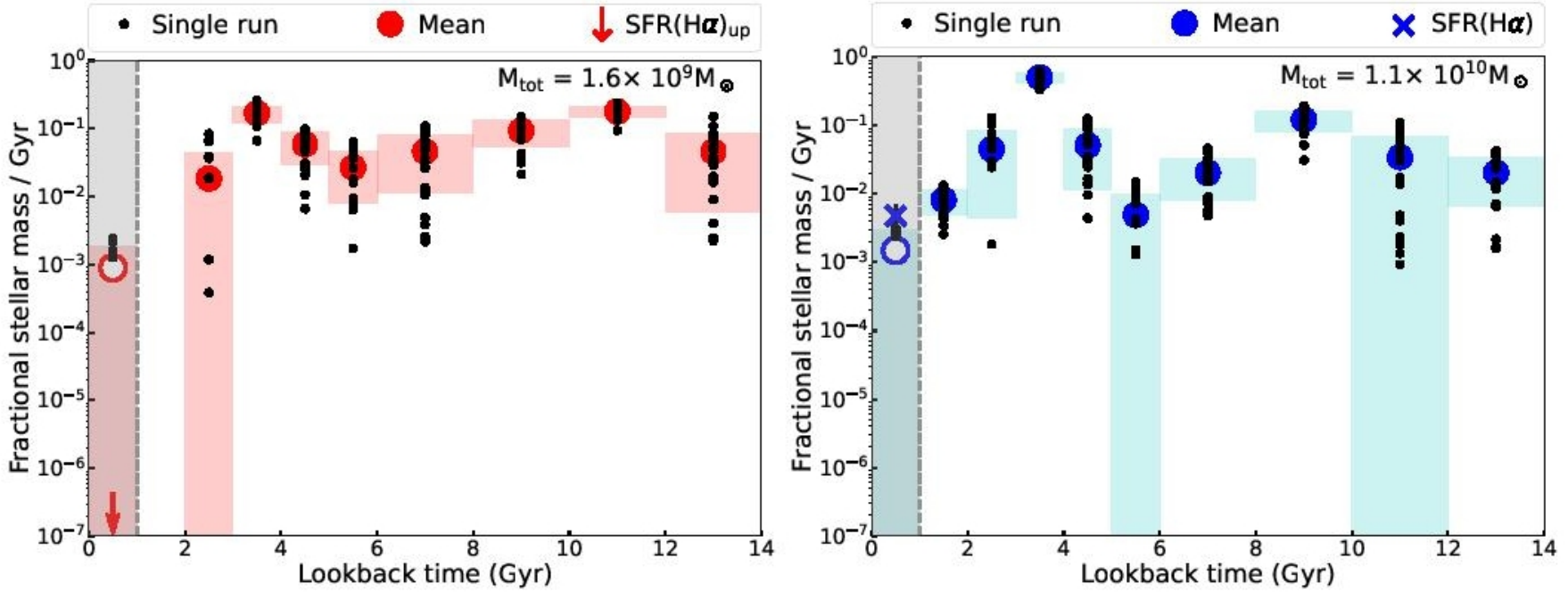

Figure 8. Final normalised SFH for the quiescent (left) and the star-forming disc (right) obtained by combining the GandALF results of 20 different fit runs that *(i)* varied the order of the multiplicative polynomial correction between 6 and 15 and *(ii)* considered either the entire MILES SSP library or only SSP models older than 1 Gyr. In both panels the black dots represent the average fractional SFR obtained from the individual fit runs (the same as the large filled circles in the example shown Fig. 7. The larger filled circles and shaded regions represent the average and standard deviation of the average fractional SFR of the single runs, including those equal to 0. For the earliest age bin, where our SFH reconstruction is unreliable (open circles and shaded grey band), we uses the MUSE Hα maps to measure or place an upper limit on the present-day star-formation rate across our inner or outer disc sectors, respectively, converting these in estimate (blue cross, right panel) or upper-limits (red downward arrow, left panel) on the fractional SFR of the first 1 Gyr by assuming such an activity remained constant over this period of time. On the top right of each panel we report the total $M_\star$ subtended by our 8 outer and 18 inner disc sectors, which cover an area of 12.5 kpc^2 and 18 kpc^2, respectively.

Не смогли восстановить для последнего 1 млрд лет? Дарю идею!